REPORT DOCUMENTATION PAGE

Form Approved
OMB No. 0704-0188

1. REPORT DATE *(DD-MM-YYYY)*	2. REPORT TYPE	3. DATES COVERED *(From - To)*
08-1-2012	Final Report	Sept. 30,2008-Sept.29, 2011

4. TITLE AND SUBTITLE
Experimental Investigation of the Plasma Bullet and Its Applications

5a. CONTRACT NUMBER

5b. GRANT NUMBER
FA9550-08-1-0487

5c. PROGRAM ELEMENT NUMBER

6. AUTHOR(S)
Dr. Mounir Laroussi, P.I.

5d. PROJECT NUMBER

5e. TASK NUMBER

5f. WORK UNIT NUMBER

7. PERFORMING ORGANIZATION NAME(S) AND ADDRESS(ES)
Old Dominion University

ODURF
4111 Monarch Way, Suite 204
Norfolk, VA 23508

8. PERFORMING ORGANIZATION REPORT NUMBER

9. SPONSORING / MONITORING AGENCY NAME(S) AND ADDRESS(ES)
Air Force Office Of Scientific Research
875 North Randolph St.
Suite 325, Rm.3112
Arlington, VA, 22203-1768

10. SPONSOR/MONITOR'S ACRONYM(S)
AFOSR

11. SPONSOR/MONITOR'S REPORT NUMBER(S)
AFRL-OSR-VA-TR-2012-0883

12. DISTRIBUTION / AVAILABILITY STATEMENT

Unlimited

13. SUPPLEMENTARY NOTES

14. ABSTRACT
This document is our final technical report describing the research activities carried out under AFOSR Grant FA9550-08-1-0487. In our previous progress reports we described the experimental device that generates the plasma bullets. Then we presented spectroscopic as well as fast photography diagnostic results that shed new light on the mechanisms of creation and propagation of the plasma bullets. We then expanded our investigations on the nature and propagation characteristics of the bullets. We also described preliminary results on a new exciting biomedical/biochemical application of the plasma bullets: The destruction of amyloid fibrils forming proteins. In this final report we add a description of new experiments that we conducted in the last year of the project. The focus of these experiments is the study of the behavior of the plasma bullets under controlled pressures and the conditions under which a large volume diffuse plasma can be ignited.

15. SUBJECT TERMS
Glow discharge, Atmospheric pressure, air plasma, plasma bullet, non-equilibrium

16. SECURITY CLASSIFICATION OF:			17. LIMITATION OF ABSTRACT	18. NUMBER OF PAGES	19a. NAME OF RESPONSIBLE PERSON
a. REPORT	b. ABSTRACT	c. THIS PAGE	Unlimited		Dr. John Luginsland
Unclassified	Unclassified	Unclassified			19b. TELEPHONE NUMBER *(include area code)* (703) 696-8574

Table of Contents

Contents

Abstract

This document is our final technical report describing the research activities carried out under AFOSR Grant FA9550-08-1-0487. In our previous progress reports we described the experimental device that generates the plasma bullets. Then we presented spectroscopic as well as fast photography diagnostic results that shed new light on the mechanisms of creation and propagation of the plasma bullets. We then expanded our investigations on the nature and propagation characteristics of the bullets. We also described preliminary results on a new exciting biomedical/biochemical application of the plasma bullets: The destruction of amyloid fibrils forming proteins. In this final report we add a description of new experiments that we conducted in the last year of the project. The focus of these experiments is the study of the behavior of the plasma bullets under controlled pressures and the conditions under which a large volume diffuse plasma can be ignited.

Introduction

One of the attractive features of non-thermal atmospheric pressure plasmas is the ability to achieve enhanced gas phase chemistry without the need for elevated gas temperatures. This attractive characteristic recently led to their extensive use in applications that require low temperatures, such as in material processing and in biomedical applications [1] – [4]. Various discharge sources capable of generating stable and relatively homogeneous plasmas at or around atmospheric pressure have been developed and characterized in recent years [5] – [6]. Many of these plasma sources use a barrier-like approach and all of them produce plasmas that are either geometrically confined to the area between the electrodes or contained within some sort of chamber or containment enclosure. Although this is very useful in several applications, there are cases where it is more desirable if the plasma were launched outside to an area not bound by anything. Plasma jets or plumes fill exactly such a niche.

Background

The Plasma Pencil

The electron energy distribution in non-equilibrium discharges plays the most important role in defining the chemistry in the plasma. It is through electron impact excitation and ionization that the charged particles, excited species, and radicals are produced. Increasing the electrons number density and their energy translates to an increase in the production of reactive species and UV radiation emission. To achieve this increase of ionization and to extend the electron energy distribution to higher values, short high voltage pulses will be used. Using short duration pulses has the advantages of keeping a low average power and not substantially increasing the gas temperature.

Nanoseconds high voltage pulses can be used to generate stable cold plasma jets. Laroussi and co-workers developed such a device, which they used for biomedical applications [7], [8]. It consists of two electrodes, each made of a thin copper ring attached to the surface of a centrally perforated alumina (Al_2O_3) disk. The hole in the center of the alumina disk is 3 mm in diameter, while the diameter of the disk is about 2.5 cm. The diameter of the copper ring is greater than that of the hole but smaller than that of the disk. The two electrodes are inserted in a dielectric cylindrical tube of about the same diameter as the disks and are separated by a gap the distance of which can be varied in the 0.3–1 cm range. Figure 1 is a schematic of the device. The two electrodes are connected to a high voltage pulse generator capable of producing pulses with amplitudes up to 10 kV, pulse widths variable from 200 ns to dc, and with a repetition rate up to 10 kHz. The rise and fall times of the voltage pulses are about 60 ns.

When a gas such as helium or argon is injected at the opposite end of the dielectric tube and the sub-microsecond high voltage pulses are applied to the disk electrodes, a discharge is ignited in the gap between the electrodes and a plasma plume/jet is launched through the hole of the outer electrode and in the surrounding room air. Figure 2 is a photograph of the device in operation. Laroussi & Lu reported jet/plume lengths of up to 5 cm and a plume gas temperature of 290 ^{o}K (Laroussi & Lu, 2005, [7]).

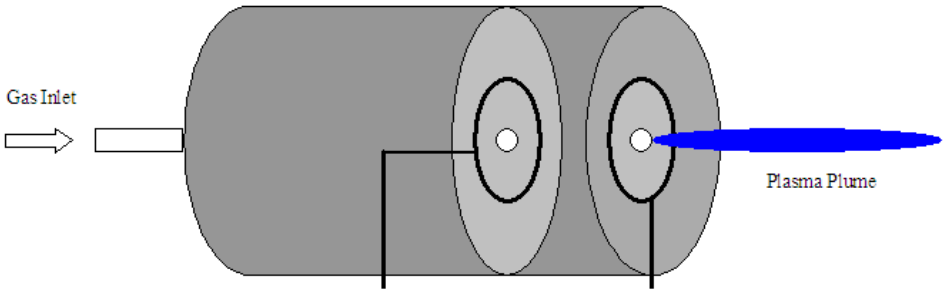

Fig. 1 Schematic of the Plasma Pencil

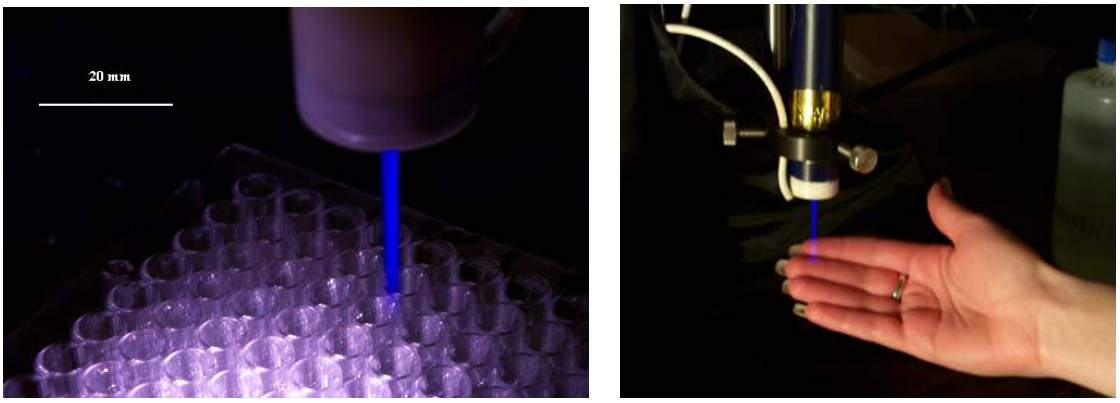

Fig. 2 Photographs of the Plasma Pencil in operation

Using fast photography Laroussi & co-workers showed that the plume is in fact a small volume of plasma, a " plasma bullet" traveling at very high velocity (see Figure 3) which exceed the gas velocity and that of any possible drift of the charges particles. Investigations (modeling and experimental) on the nature of this plasma bullet and its propagation are only starting. The following section presents measurements that shed some light on this fascinating process and the role of nanoseconds high voltage pulses in triggering and sustaining such exotic plasma.

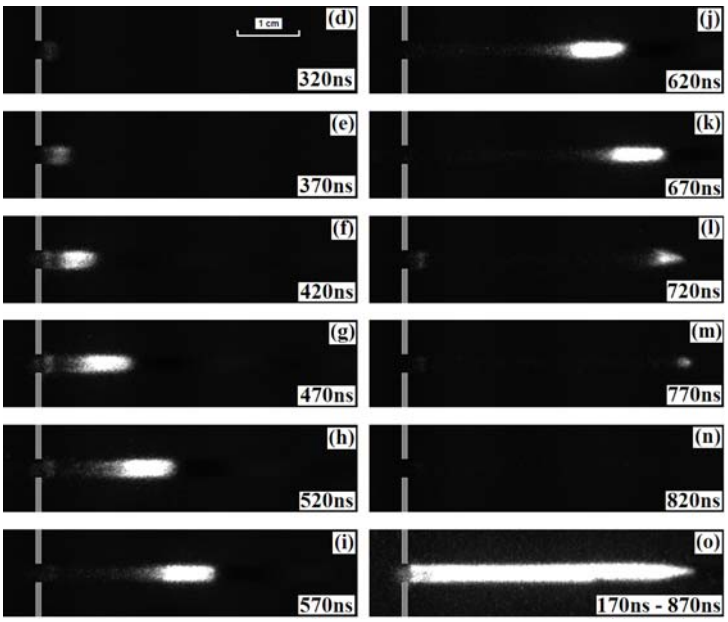

Fig. 3 Pictures taken by ICCD camera showing the plasma bullet as it travels forward in the surrounding air.

Results and Discussion (Year 1)

The dynamics of the plasma bullet were captured using a high-speed Intensified Charge Coupled Device (ICCD) camera (DiCam Pro) with exposure times of a few nanoseconds. The bullet starts to accelerate as soon as it is launched from the hole of the outer electrode. At some distance it reaches its maximum velocity and then the velocity drops quickly until the bullet cannot be captured by the ICCD anymore. The maximum value of the plasma bullet velocity is in the order of 10^5 m/s, a much greater value than the gas velocity of 8.3 m/s, as calculated according to the gas flow rate and the diameter of the hole.

To further understand and characterize the plasma bullets, ICCD imaging and spatially resolved emission spectroscopy are used to investigate the propagation of the bullet, reveal its structure, and follow the evolution of its important chemical species, such as O, N_2, N_2^+, and OH. The parameters influencing the characteristics of the bullet are identified, pointing the way to the possible physical processes responsible for the creation of these bullets.

Figure 4 shows pictures of the discharge inside the discharge chamber (between the electrodes) and that of the bullet at different times, as captured by the DiCamPro ICCD camera. As seen in Figure 4, a first discharge is observed in the discharge chamber. This discharge occurs around the time the voltage pulse reaches its plateau (See Figure 5). This discharge is accompanied with a first current peak. 120 ns after the occurrence of this peak a bullet is launched out of the chamber and into the ambient air. The launch of the bullet comes with a second current pulse that is much weaker than the previous one. When the voltage falls, a second discharge is ignited inside the chamber and is accompanied by a negative current pulse. It is at this time that the bullet extinguishes. Therefore, the propagation of the plume is only sustained during the voltage pulse. This was confirmed by changing the pulse width and finding that the extinction of the bullet always occurred at the end of the applied voltage pulse.

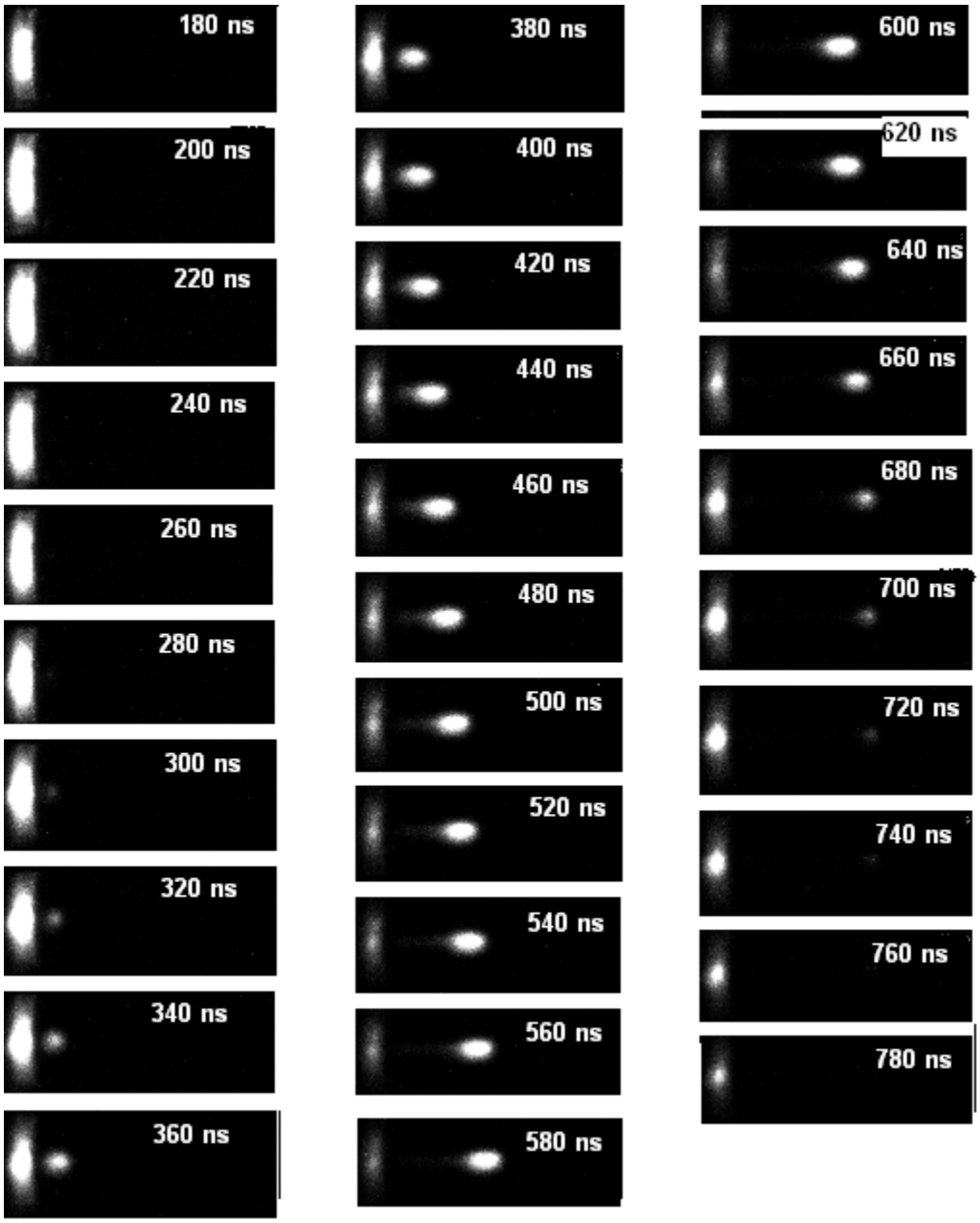

Fig. 4 High-speed photographs of the discharge and the bullet emitted by the plasma pencil. Exposure time of the camera is 50 ns. V = 5 kV, pulse width is 500 ns.

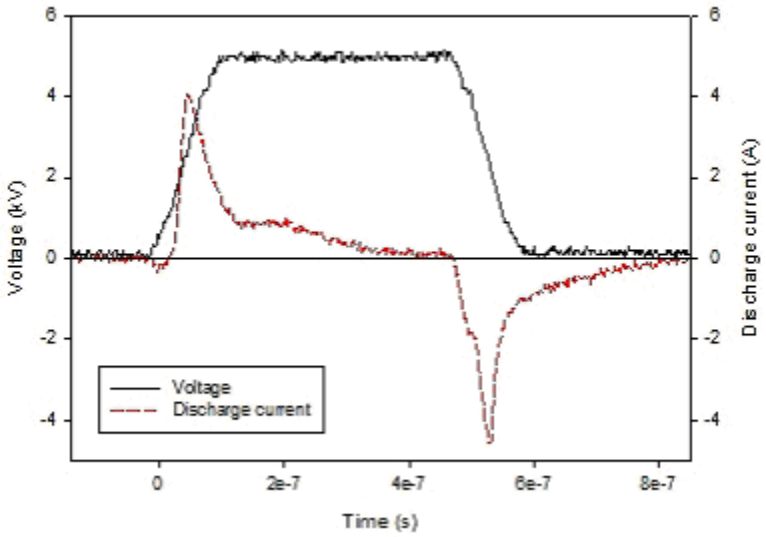

Fig. 5 Current-Voltage Charateristics

Another interesting observation is the fact that regardless of the magnitude of the applied voltage pulse, the bullet extinguishes at the same time, which also corresponds to the fall of the pulse. Figure 6 illustrates this observation. Figure 6 also shows that when the voltage increases, the average bullet velocity increases also. The shape of the curve remains the same, but the maximum velocity is reached earlier for higher voltages. Most interestingly, as the voltage increases the bullets formation occurs at earlier times with the extinguishing time remaining the same, as mentioned earlier. Therefore, in order to reach the end of its trajectory always at the same time, both the average velocity of the bullet and its formation time appear to change accordingly: earlier formation time and reaching higher velocities for increasing voltages. It is important to mention here that the velocity of the bullet is several order of magnitudes higher that the gas velocity out of the device. Figure 7 shows the gas velocity (flow rate of 7.7 l/min) as a function of distance as measured by a Pitot tube. Figure 7 also shows that the spatial dependence of the gas velocity is quite different than that of the plasma bullet.

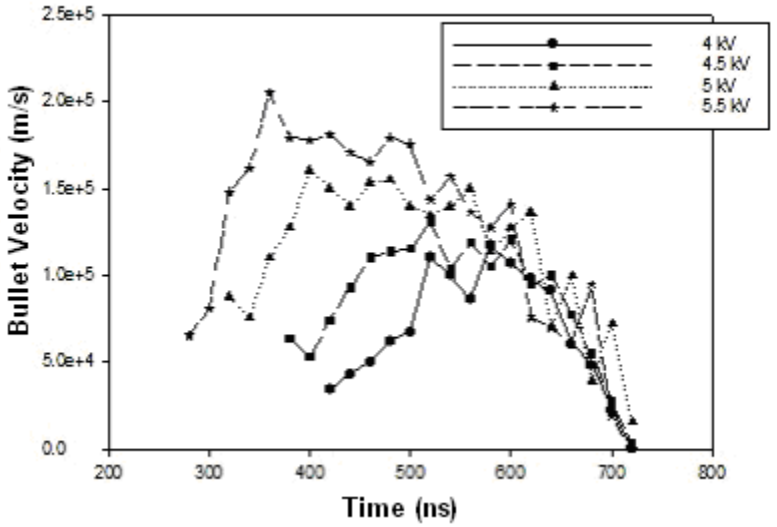

Fig. 6 Bullet velocity versus time for different voltages, helium flow rate around 7 l/min. Pulse width is 500 ns.

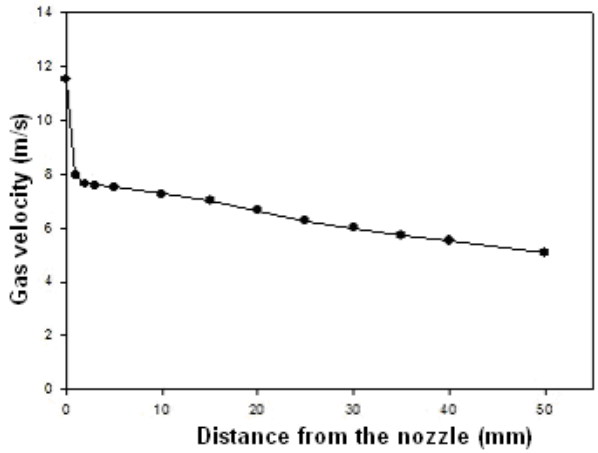

Fig. 7 Gas velocity along the axis for a flow rate of 7.7 l/mn.

To reveal accurate features of the structure of the bullets, the ICCD camera was placed both at an angle and also head-on with respect to the plasma plume. It turned out that the bullet is in fact hollow and has a “donut” structure. This is a very important observation as it supports the idea that the plasma bullet in fact propagates along the interface of two media, the helium channel and the ambient air. This leads to the proposal that the bullet is a solitary ionization surface wave. Figure 8 illustrates the donut shape of the bullets.

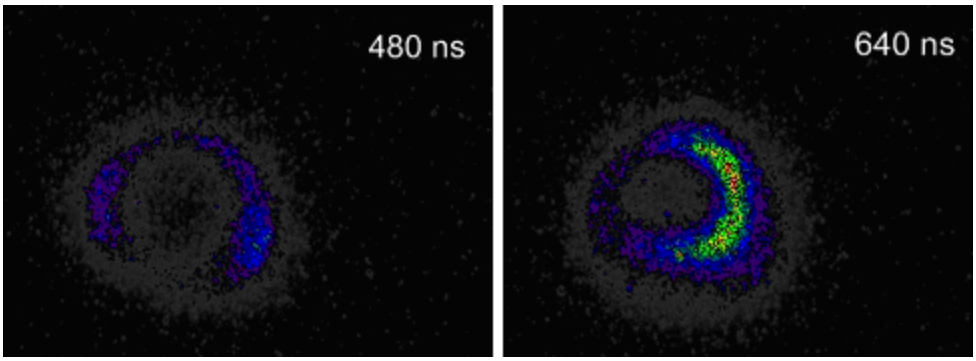

Fig. 8 Photographs of the bullets illustrating their donut shape.

Optical Emission Spectroscopy

Optical Emission Spectroscopy was used to identify the chemical species present in the plasma plume. Figure 9 shows the experimental setup.

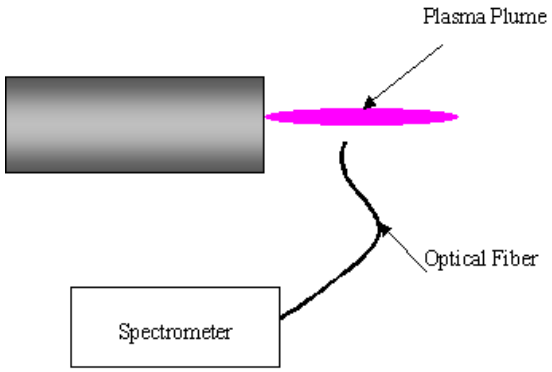

Fig. 9 Experimental setup for the spectroscopy measurements

Figure 10 shows a typical emission spectrum for a helium plasma plume in air, taken by an Ocean Optics mini-spectrometer USB4000. The emission spectrum is dominated by N_2^+ and also by N_2 excited states. Atomic oxygen, O, and OH lines are also present. To study the variation of the intensity of the main emission lines (N_2, N_2^+, O, OH, and He) we used an optical fiber to collect the localized emission along the axis of the plume. Figure 11 shows the intensities of these emission lines as a function of the flow rate (collected at an axial distance of 8 mm from the outer aperture of the device) and Figure 12 their intensities as a function of distance along the plume axis (gas flow rate of about 7 l/min). The intensity curve of N_2^+ is particularly interesting: The N_2^+ line intensity reaches a maximum value at the same flow rate (~7 l/min) under which a maximum plume length is achieved. This is an indication that the N_2^+ density is a crucial parameter influencing the physical characteristics of the plume. Of note also is the fact that the helium line follows the same behavior with a maximum at the 7 l/min flow rate. Figure 12 shows that the N_2^+ and He lines intensities exhibit optima around 12 mm from the beginning of the plume. This position happens to be around the same position where the bullets reach their

maximum velocity. This fact seems to indicate that N_2 ionization by helium metastable states may play an important role in the propagation mechanism of the plume/bullets.

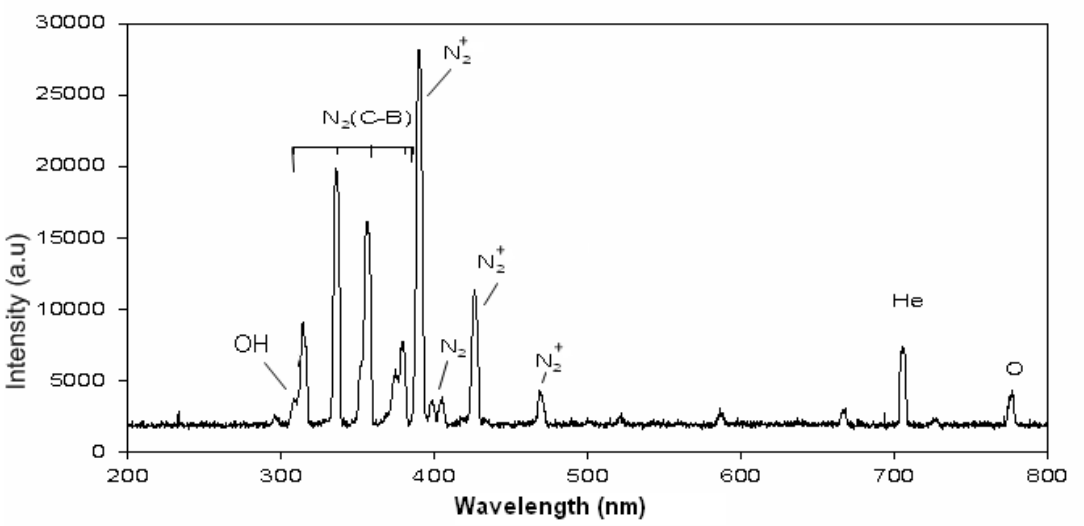

Fig. 10 Typical emission spectrum from a helium plume emitted in ambient air. V = 5 kV and pulse width is 500 ns.

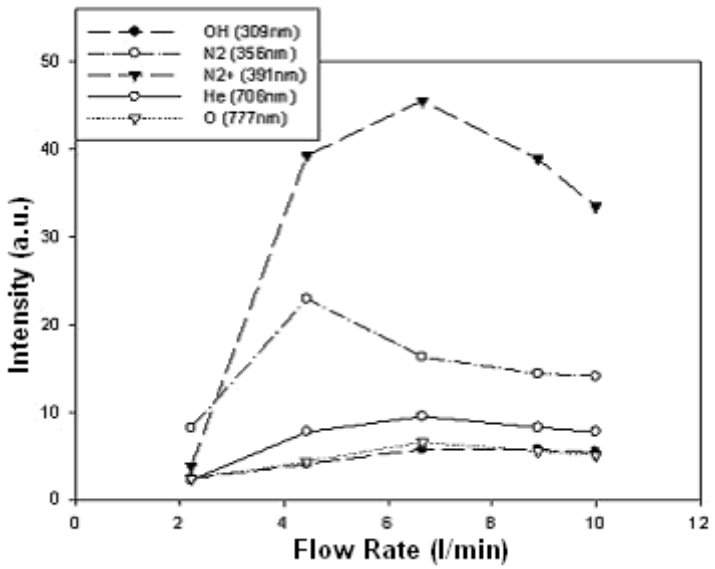

Fig. 11 Intensities of selected emission lines as a function of gas flow rate. Light is collected at 8 mm from the beginning side of the plume. V = 5 kV and pulse width is 500 ns.

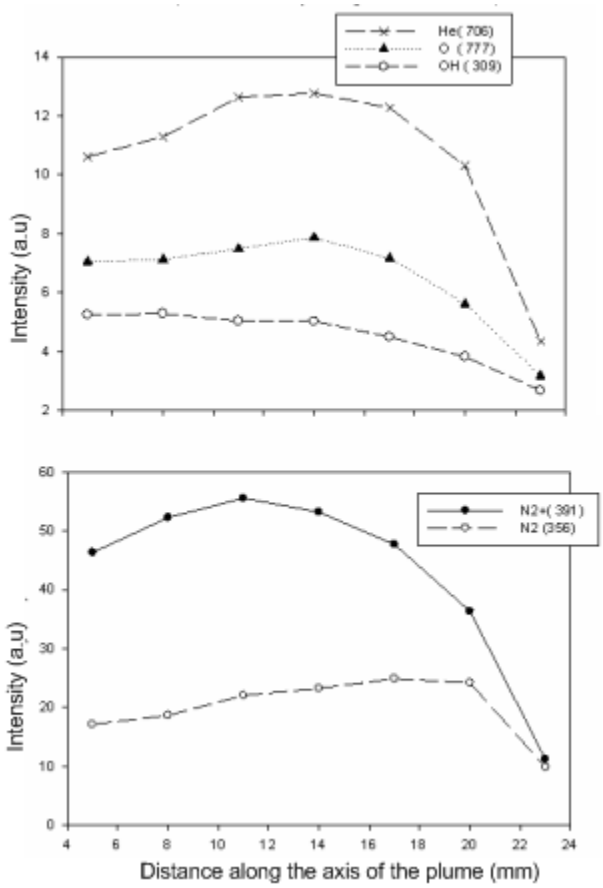

Fig. 12 Intensities of the He, N_2, N_2^+, O, and OH emission lines as function of the axial distance from the beginning side of the plasma plume. Gas flow rate is 7 l/min. V = 5 kV and pulse width is 500 ns.

Work on furthering our investigations on the dynamics of the plasma bullet is underway. These investigations are looking into the role of gas flow and helium mole fraction in the propagation of the bullet. Both experimental and simulation work are carried out simultaneously to attempt to explain how the bullets form and why they are donut-shaped. Results will be reported in due time.

New Results (2009-2011)

Determination of the bullet lifetime

Figure 13 shows the experimental setup used for this study. Note that the plasma bullet lifetime is related to the plasma jet length since the plasma jet is the footprint of the plasma bullets.

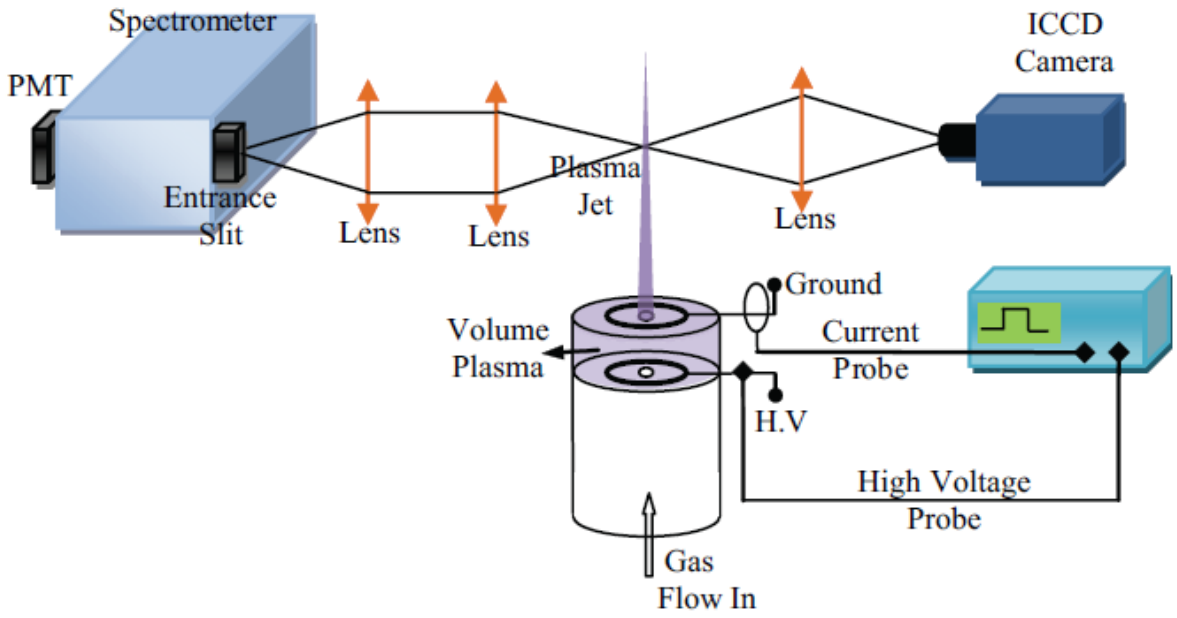

Fig. 13 Experimental setup

The plasma bullet lifetime depends on the helium mole fraction along the propagation path, the magnitude of the applied voltage, and the secondary discharge ignition time. In dielectric barrier discharge (DBD) sources that are driven by short high voltage pulses, Laroussi and co-workers showed that in addition to the main discharge a secondary discharge is self-ignited during the fall-time of the applied high voltage pulse. The secondary discharge occurs at the end of the applied high voltage pulse due to the charge accumulation established by the primary main discharge on the surface of the dielectric.

For a pulse width less than a certain value, the plasma bullet stops propagating just after the secondary discharge ignition. The reason for this interesting phenomenon will be investigated later in this paper. The ionization channel contains short-lived, such as He^*, N_2^*, N_2^* , and long-lived, such as He^m (helium metastables), O_3, NO, NO_2, reactive species. The zones, where the propagation of the plasma bullet is inhibited by low helium mole fraction or secondary discharge ignition, are shown in Figure 14. If the pulse width is long enough, the plasma bullet propagation is inhibited before the ignition of the secondary discharge due to quenching by air molecules (mostly by oxygen) diffusing into the ionization channel. This limit is called the transition point that separates the plasma bullet inhibition zones (the secondary discharge ignition zone from low helium mole fraction zone) as seen in Figure 14. This transition point shifts as a function of the applied voltage from 1300 ns to 425 ns (Figure 15) since the plasma bullet is able to arrive to this transition point earlier at higher applied voltages due to its higher velocity.

This transition point is important for the optimum operating conditions of the plasma pencil. How the plasma bullet comes to an end affects the structure of the tip of the plasma plume. If the secondary discharge ignition inhibits the propagation of the plasma bullet, the plasma plume tip is shaped as a sharp and homogenous structure. In contrast, in the case of low helium mole fraction, the plasma jet tip seems inhomogeneous and is unstable. In applications, such as material processing or biomedicine, the condition of the tip of the plasma plume is very important since it is the part that comes in contact first with the surface under treatment.

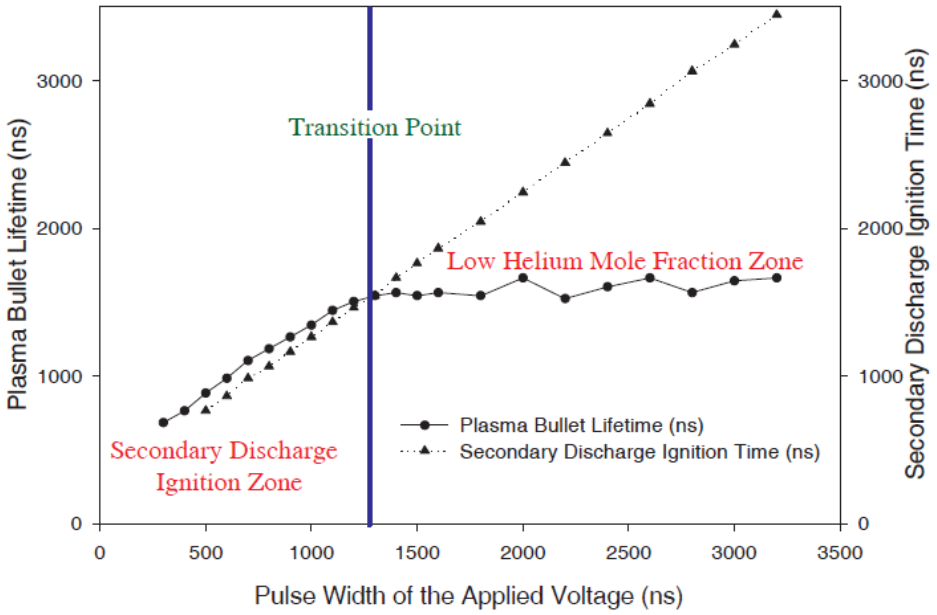

Fig. 14 Plasma bullet lifetime as a function of the pulse width (Applied Voltage: 4 kV; Repetition Rate: 5 kHz; Flow Rate: 5.0 L/min).

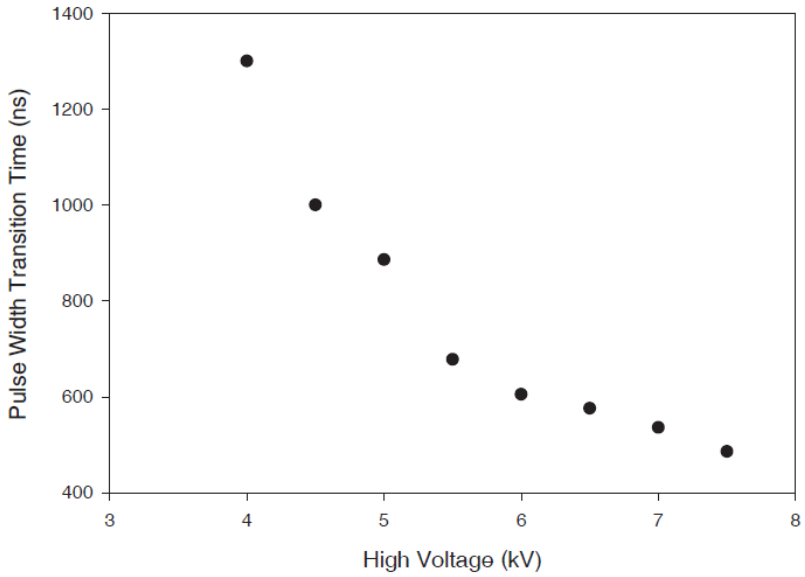

Fig. 15 The pulse width transition time as a function of the applied voltage (Repetition Rate: 5 kHz; Flow Rate: 5.0 L/min).

A. Influence of the helium mole fraction and applied voltage

To sustain the plasma bullet propagation a minimum density of helium atoms is required in the propagation channel. This amount can be quantitatively represented by the helium mole fraction. The helium flow passing through the electrodes controls the length and homogeneity of

the plasma jet. The plasma jet length for different helium flow velocities was measured, and then the minimum corresponding helium mole fraction at the tip of the plasma jet was extracted from the helium flow simulation results. This simulation was performed by a commercially available partial differential equation solver (COMSOL Multiphysics 3.4). Another factor, the magnitude of the applied voltage (the applied energy), is also of consequence. How much applied voltage is needed to initiate the plasma bullet formation (i.e. how much energy is transferred into the ionization channel) is an important parameter because the plasma bullet dissipates its energy as it propagates forward. It was found that the helium mole fraction and applied voltage should be more than a critical value along the plasma bullet propagation path to sustain the plasma chemistry in the plasma bullets.

B. Secondary discharge ignition

As the plasma bullet propagates further, it leaves behind an ionization channel consisting of short-lived and long-lived reactive species. This is supported by ICCD camera photographs shown in Figure 16 and temporal OES data shown in Figure 17.

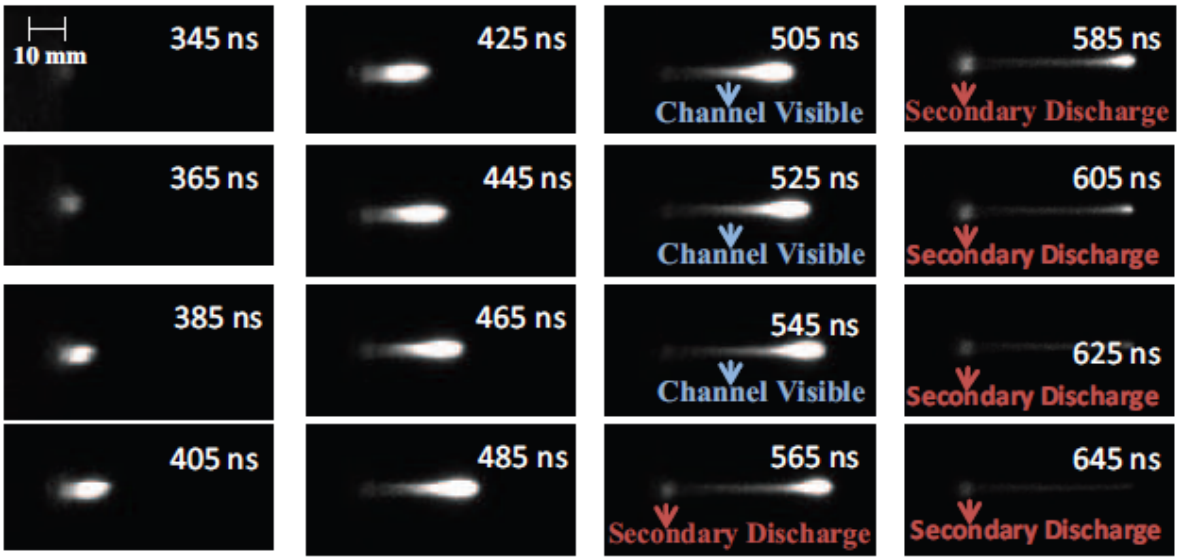

Fig. 16 The plasma bullet propagation showing the channel consisting of emitting species along the ionization channel. Secondary discharge ignition causing the plasma bullet inhibition (Applied voltage: 5.5 kV; Pulse width: 300 ns; Repetition rate: 5 kHz; Flow Rate: 5.0 L/min).

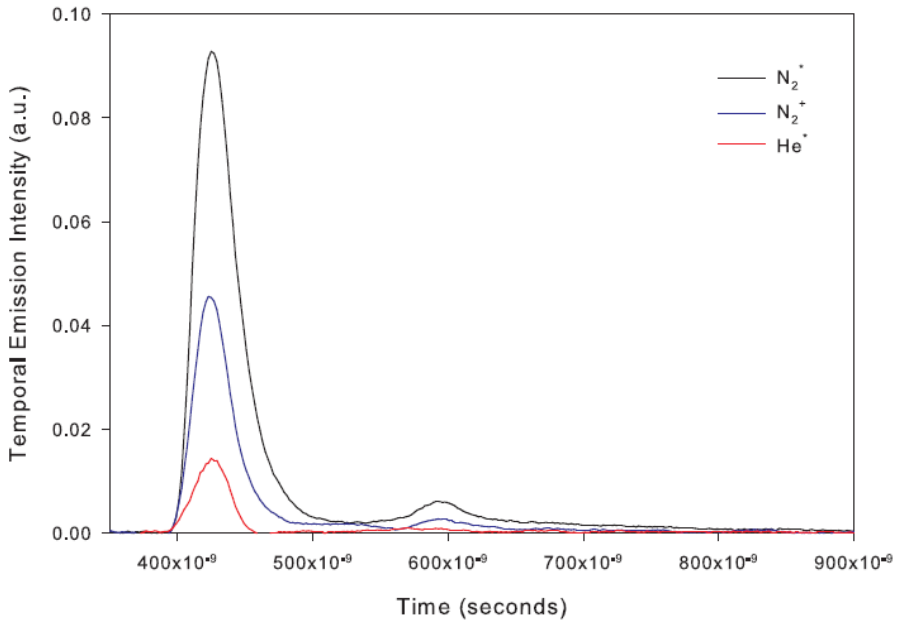

Fig. 17 Temporal evolution of the reactive species at 20 mm away from the plasma pencil (Applied voltage: 5.5 kV; Pulse width: 1000 ns; Repetition rate: 5 kHz; Flow Rate: 5.0 L/min).

Our current experimental setup allows identifying only emitting species associated with short-lived species along the ionization channel. The temporal evolution of the emitting species provides an insight into the constituents of the channel. During the experiments, the focal point of our lens is 20 mm away from the plasma pencil. Basically, as the plasma bullet passes through this focal point, the distribution of the emitting species is recorded by the monochromator. As shown in Figure 17, the magnitude of the emission intensity first increases and eventually reaches its highest value. This region corresponds to the point where the ionization front propagates forward. Then, the emission decreases exponentially until it reaches low emission levels. This proves that even though the ionization front moves 50-60 mm away from the plasma pencil, it leaves behind short-lived reactive species which remain at low concentration values along the ionization channel.

The channel initially appears as an extension of the plasma bullet. If the applied voltage is sufficiently high, the plasma bullet eventually breaks off this extension. The time when the plasma bullet breaks off is determined as a function of the applied voltage. This break-off time corresponds to a point when the short-lived reactive species are at very low concentrations making them invisible to the ICCD camera (The ICCD camera can track emissions between 200 nm - 900 nm wavelengths). It is found that the plasma bullet breaks off faster at higher voltages (Figure 18). This is due to the faster velocity of the plasma bullet at higher voltages. However, this break-off time is independent of the pulse width.

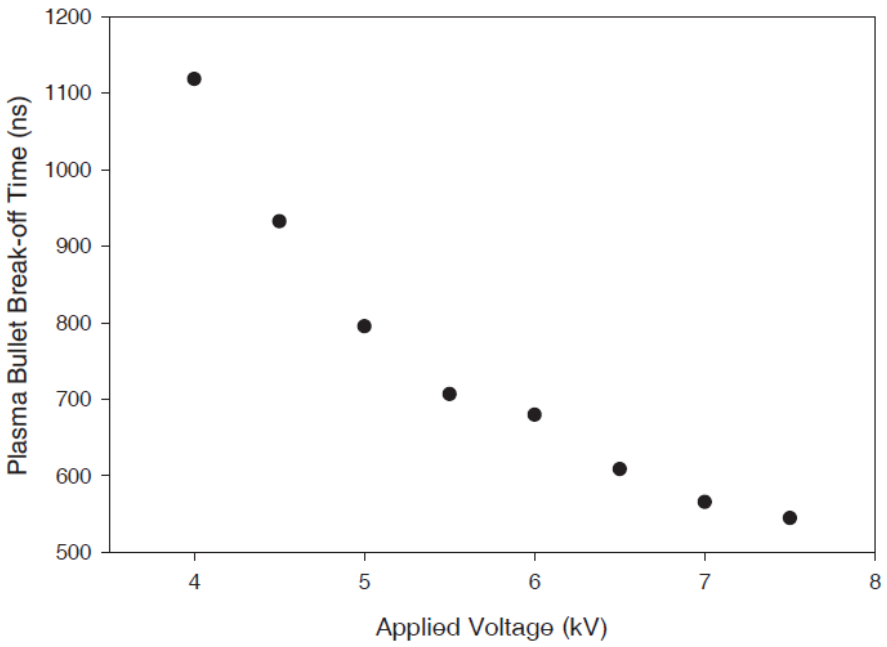

Fig. 18 Plasma bullet break-off time for different applied voltages (Pulse width: 2000 ns; Repetition rate: 5 kHz; Flow Rate: 5.0 L/min).

Even when the plasma bullet breaks off, the secondary discharge ignition (initially occurring inside the device) is still able to inhibit the propagation of the plasma bullet. This supports the idea that long-lived species exist throughout the ionization channel along with low concentrations of short-lived species, which helps the outward expansion of the secondary discharge. Therefore, the secondary discharge initially ignited at the dielectric electrode surface propagates along the ionization channel, and then stops the plasma bullet from propagating in an abrupt manner. In order to observe the secondary discharge propagation, the operating conditions of the plasma pencil are set to 7 kV applied high voltage and 2800 ns pulse width, which allow for an easy observation of the secondary discharge during its propagation. In addition, the 2800 ns pulse width provides for a good separation of this propagation from that of the plasma bullet, and eliminates the contribution of the short-lived species along the ionization channel. Figure 19 shows that the secondary discharge also travels in the air up to 40 mm away from the reactor. Therefore, it is deduced that the secondary discharge ignition creates another propagation in the surrounding air.

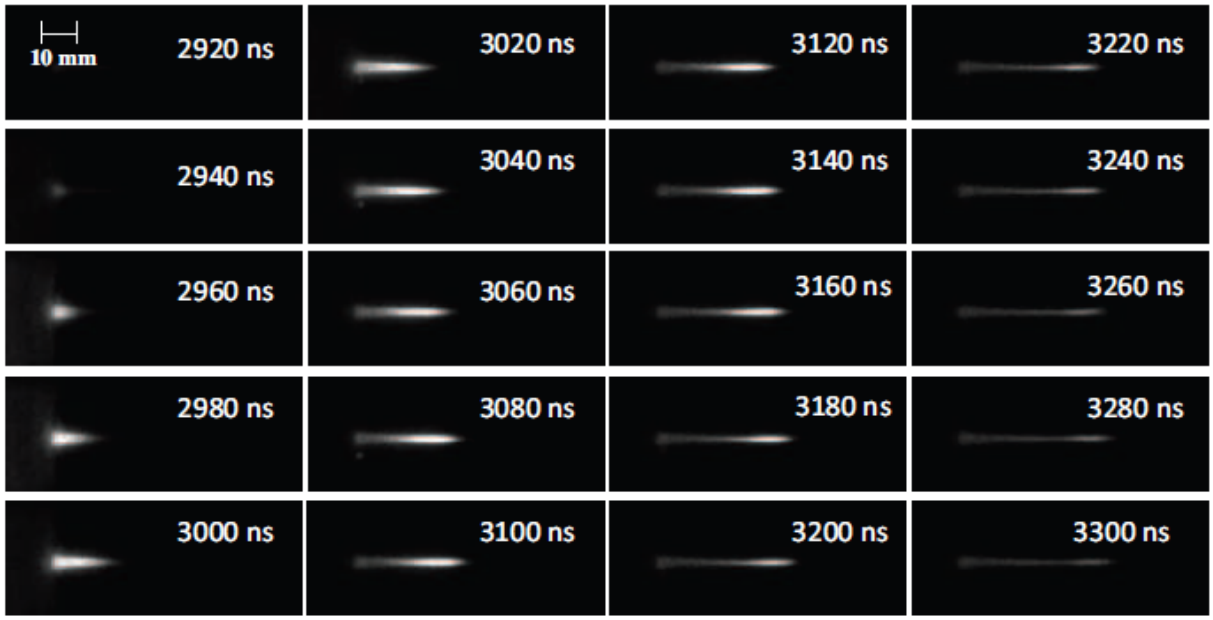

Fig. 19 Secondary discharge propagation at 7 kV applied voltage and 2800 ns pulse width.

The secondary discharge effect on the plasma bullet inhibition can be explained by our recent experimental observations. Based on these observations, it is confirmed that the plasma bullets adopt the streamer propagation mechanism. These observations show that the plasma bullets generated by positive applied voltages travel similarly as in the case of the cathode-directed streamers. In this streamer mechanism, the electron flow is opposite to the direction of propagation of the plasma bullet. It is also found that during the propagation a number of the electrons accumulate onto the positive electrode dielectric surface. The electron number in this accumulation is almost equal to the electron number in the plasma bullet. When these electrons are released from the dielectric surface at the end of the applied voltage pulse, they create an opposing current along the ionization channel. Therefore, this "negative current", acting against the normal succession of events during the bullet propagation, leads to slowing down of the plasma bullet and then eventually its inhibition. This mechanism needs further detailed investigations and will be reported in the future.

Characterization of the plasma bullet velocity by emission spectroscopy

Measurement of the plasma bullet velocity is an important and necessary task for the investigations of the dynamics of the plasma bullet propagation. High-speed photography based on the use of ICCD cameras allows observing the plasma dynamics in time domain with resolutions as low as a few nanoseconds. Although this technique is unique, the resolution of the ICCD cameras is not high enough for the plasma bullet velocity to be measured in detail.

In our previous work, the instantaneous plasma bullet velocity was determined by an ICCD camera with a resolution of 20 ns. This resolution is not enough to elucidate the detailed behavior of the plasma bullet during its propagation in the surrounding air. In previous work, it was reported that the plasma bullet starts its propagation with relatively lower velocities, and then it reaches its maximum. As it travels further, its velocity decreases. Finally, at the end of the applied voltage pulse, the plasma bullet stops propagating. Unfortunately, Fluctuations in the

instantaneous plasma bullet velocity plagued the measurements in that study. Although the resolution of the ICCD cameras could be as low as 3 ns in theory, an exposure time of around 20 ns is usually needed to collect a sufficient amount of photons in order to observe the plasma bullet. In addition, a precise protocol is necessary to identify a reference point in order to measure the distance from the plasma bullet to the reactor. This rendered the task particularly difficult and required the use of advanced image processing technique.

In the present study, a time-resolved OES is applied to the measurement of the plasma bullet velocity with a resolution as good as 0.5 ns. Figure 17 shows the temporal evolution of the reactive species at 20 mm away from the plasma pencil for the applied voltage of 5.5 kV with a 1μs pulse width. Spectral lines for these reactive species are as follows: N_2* (second positive system (SPS)): 337.1 nm line of $C^3\Pi_u \rightarrow B^3\Pi_g$ g, N_2^+ ; (first negative system (FNS)): 391.4 nm line of $B^2\Sigma_u^+ \rightarrow X^2\Pi_g^+$, and He*: 706.5 nm line. The chosen lines are determined in terms of the magnitude of emissions in their spectral systems.

Based on Figure 17, the reactive species emit their highest peaks at around 425 ns. The occurring time of these peaks depends on the magnitude of the applied voltage and the focusing position of the lenses along the plasma jet. For example, at further spatial points the highest peak occurs later, or with higher applied voltages the highest peak occurs earlier. The former is illustrated in Figure 20. In this technique, these shifts will be basically utilized for the measurement of the plasma bullet velocity.

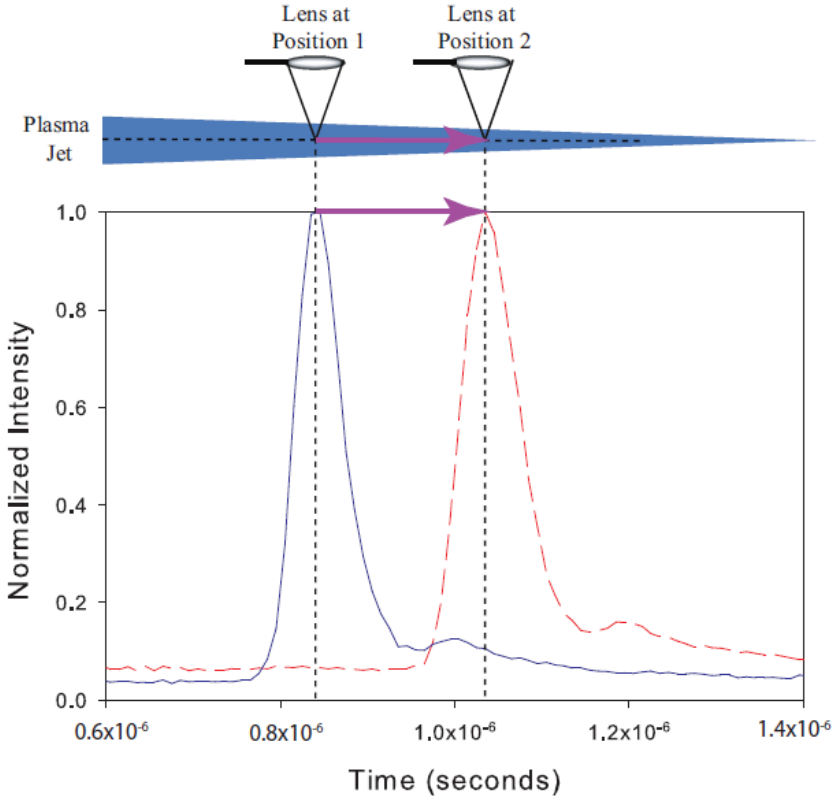

Fig. 20 Evidence of a shift of the highest emission peak for the plasma bullet velocity measurements.

The average and instantaneous plasma bullet velocities are measured from the temporal evolution of the reactive species. The emitted light is collected along the plasma jet, and is

monitored on a wideband oscilloscope. The time that the plasma bullet propagates in the air (i.e. time of the highest peak of the reactive species emission) is measured at the peak of the temporal evolution of the reactive species. The distance to the plasma pencil is precisely measured by an adjustable micrometer.

The average plasma bullet velocity is calculated at the peaks of N_2*, N_2^+, and *He** temporal emissions as a function of the applied voltage. The launching time of the plasma bullet is determined by an ICCD camera, and then it is subtracted from the time of the highest peak in order to calculate the average plasma bullet velocity more accurately. It is found that the average plasma bullet velocity increases as the applied voltage increases (Figure 21). In addition, identical average plasma bullet velocity is obtained from the emission of different reactive species for each applied voltage.

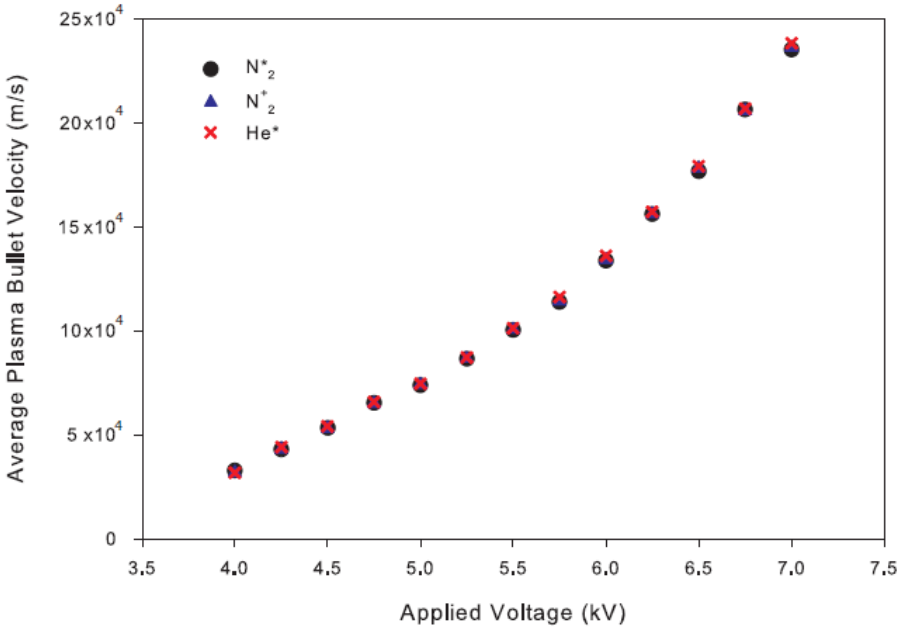

Fig. 21 The average plasma bullet velocity for different reactive species as a function of the applied voltage (Pulse width: 2000 ns; Repetition rate: 5 kHz; Flow Rate: 5.0 L/min).

The instantaneous plasma bullet velocity is calculated from the consecutive temporal emissions of N_2* (SPS) at 337.1 nm along the plasma jet since N_2* (SPS) at 337.1 nm is one of the strongest emissions along the plasma jet. Each consecutive measurement is done by only one PMT (only the focal point is displaced by a micrometer). The oscilloscope output is averaged 500 times in order to obtain more accurate data. Therefore, the resolution of the oscilloscope allows decreasing the time error to 0.5 ns for each acquisition. As shown in Figure 22, the instantaneous plasma bullet velocity does not follow a smooth velocity curve due to the highly collisional medium of air at atmospheric pressure. However, the numerous experimental observations show a consistent pattern. The instantaneous plasma bullet velocity experiences three different phases during its travel: launching, propagation, and ending (Figure 22). The plasma bullet launches from the plasma pencil with relatively lower velocities, and then it reaches its maximum at 1.1×10^5 m/s. This increase is due to an excessive amount of nitrogen molecules in the air. After that, the plasma bullet enters the propagation phase. During the propagation, its velocity remains almost constant. At the end of the pulse, the applied high

voltage starts decreasing, and the plasma bullet comes to an end at around 70 mm in an abrupt manner. These three phases can be seen from the ICCD camera photographs in Figure 23. It is worth noting that the velocity measurements at the early beginning and late ending of the propagation are unstable (grey regions in Figure 22). In these regions, the plasma bullet is not propagating or seems to oscillate back and forth. For the early beginning, the reason of this instability is that the plasma bullet just starts being formed, and is still in contact with the reactor (i.e. the dielectric surface of the electrode). For the late ending, the plasma bullet cannot sustain the chemical reactions due to quenching of excited states by air molecules after a certain spatial point. This quenching phenomenon causes the plasma emission to faint, undergoing electron attachment and ion recombination at the end of the pulse. That point corresponds to the late ending of the plasma bullet propagation.

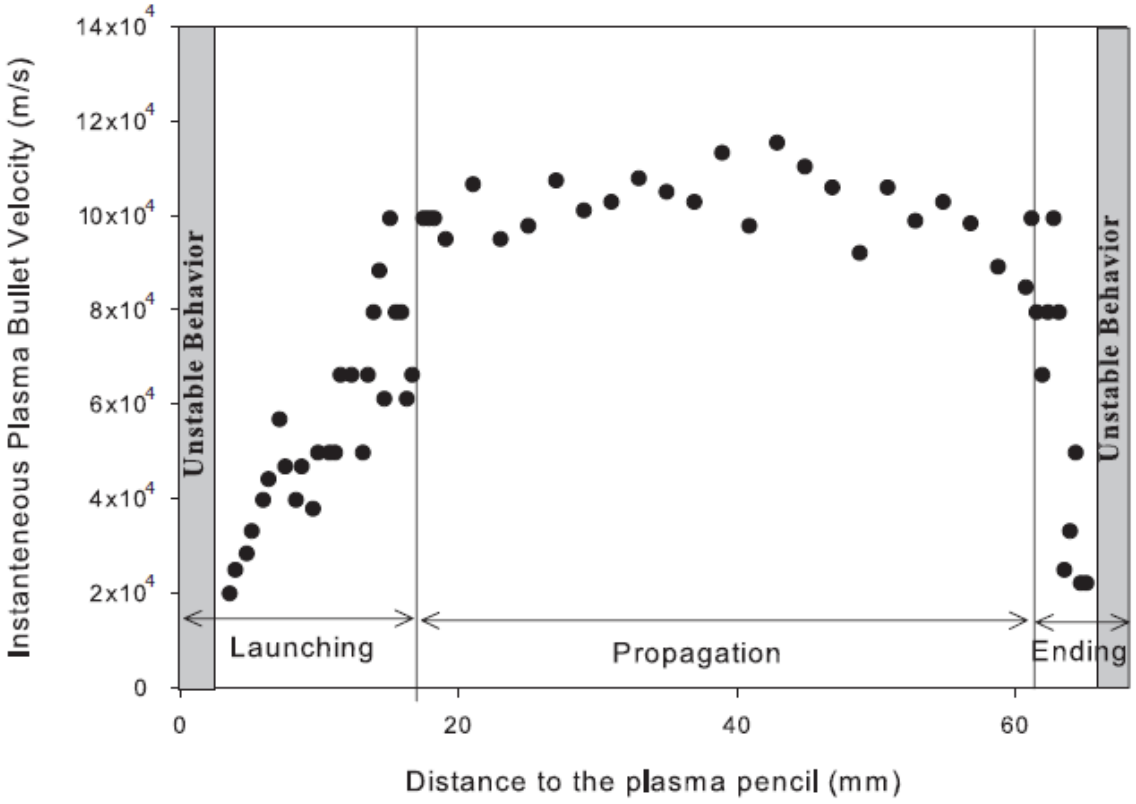

Fig. 22 The instantaneous plasma bullet velocity from the emission of SPS by a time-resolved OES (Applied voltage: 5.5 kV; Pulse width: 2000 ns; Repetition rate: 5 kHz; Flow rate: 5 L/min).

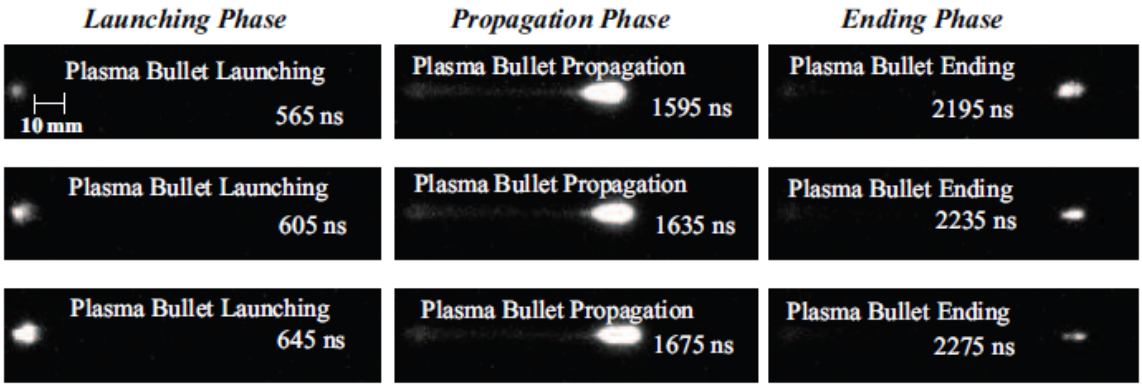

Fig. 23 Plasma bullet experiences three different phases: launching, propagation, and ending Applied voltage: 5.5 kV; Pulse width: 2000 ns; Repetition rate: 5 kHz; Flow rate: 5 L/min).

A New Application for Biochemistry: Destruction of Amyloid Fibrils

Amyloid fibrils are ordered beta-sheet aggregates that are associated with a number of neurodegenerative diseases such as Alzheimer's and Parkinson's [9]. Amyloid fibrils can also be found in other parts of the human body such as joint spaces in patients undergoing prolonged renal dialysis [10]. There are approximately twenty proteins that have been found to form fibrils in humans and are associated with disease states [9]. However, it has been postulated that all proteins can be induced to form this low energy state if subjected to the right conditions [11]. We are investigating potential methods involving the use of cold plasma that will lead to the destruction of amyloid fibrils, formed by the protein α-synuclein, which underlies Parkinson's disease and the amyloid-β peptide which is thought to be associated with Alzheimer's disease [12]. Parkinson's disease is a neurodegenerative movement disorder. It results from the degeneration of dopaminergic neurons in the substantia nigra, a region of the brain that controls movement. Death of dopaminergic neurons by the formation of amyloid fibrils with the protein α-synuclein results in decreased production of dopamine. Lack of dopamine results in the major symptoms of Parkinson's disease: rigidity to muscles constantly contracted, resting tremor, postural instability and slowness in initiating movement. Alzheimer's disease is believed to be caused by the fibrillation of a peptide called amyloid-β after it is cleaved from the precursor protein on the cell surface in the brain. The residues composing this peptide are mainly 1-42 and spontaneously form amyloid fibrils. The fibrillation, which is believed to cause Alzheimer's, begins in the temporal lobes of the brain and then spreads to other parts of the brain, thus killing cells and interfering with neural transmissions. At present there is no cure for these progressive and debilitating diseases. We propose that this work may also be applicable to the destruction of prion proteins and have value in decontamination processes.

In our experiments, the human protein α-synuclein was selected as the initial model system. It is produced by expressing it in *Eschericia coli* from a DNA clone inserted into the bacteria. The soluble protein is then extracted from the bacterial cells and purified by ion-exchange and gel filtration chromatography. The α-synuclein protein (4-6 mg/ml) is dissolved in a buffer solution of 0.2M NaCl in 20mM Tris Base, pH 7.5 and incubated at 37ºC in an incubator shaking at 150-190 rpm. After 15 days mature fibrils analogous to those in patient's brain are formed in our test tubes.

The plasma pencil was used to generate the plasma bullets that are applied directly on pre-prepared amyloid fibrils samples. The operating conditions of the plasma were the following: Voltage pulse magnitude was 7.5 kV, pulse width and frequency were 1 μs and 5 kHz respectively, and feed gas was helium at a flow rate of 5 slpm. Figure 24 is a photograph of the plasma plume.

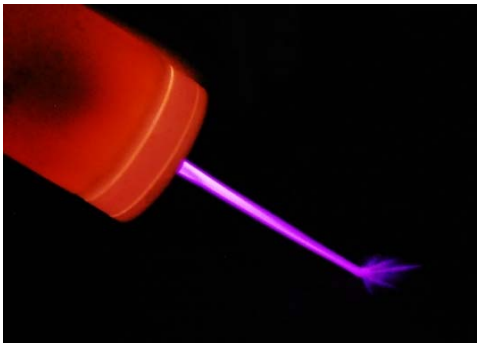

Fig. 24 Photograph of the plasma plume generated by the plasma pencil.

Figure 25 shows a spectrum of emission from the plume/bullets. It is dominated by emission lines from excited nitrogen, nitrogen molecular ions, and helium. Atomic oxygen and hydroxyl lines are also present. Figure 26 shows the spatial distributions of the important chemical species along the axial position. This information allows us to determine the optimum placement of the biological samples downstream of the plasma jet.

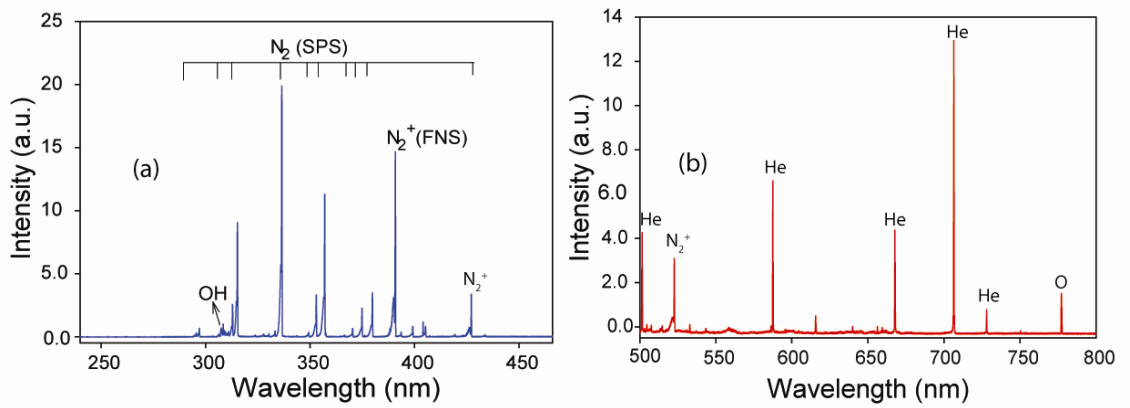

Fig. 25 (a) A typical ultraviolet (UV) emission spectrum showing emission of OH, N_2 Second Positive system (SPS), and N_2^+ First Negative System (FNS); (b) A typical visible-infrared (visible-IR) spectrum showing emission of N_2^+, He, and O (HV amplitude: 7.5 kV; pulse repetition frequency: 5 kHz; helium gas flow rate: 5 L/min; pulse width: 500ns).

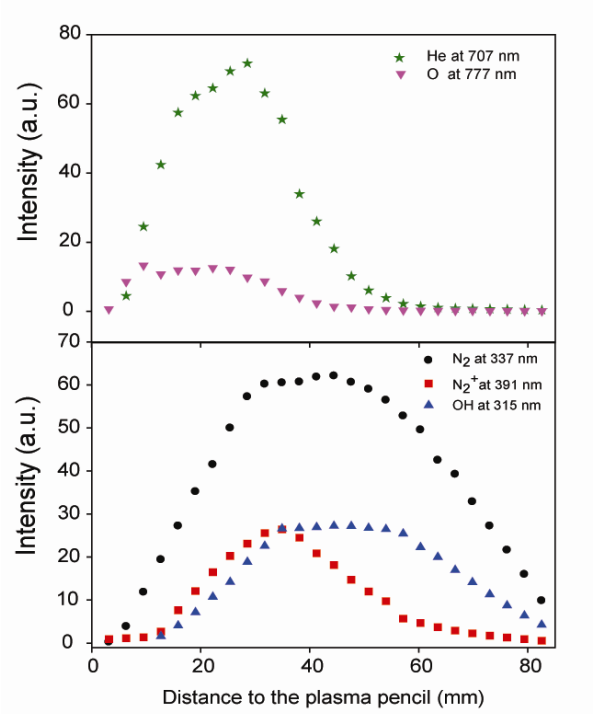

Fig. 26 Spatial distribution of the emitting species along the plasma plume showing that N_2, N_2^+, OH, and O play important roles in the plasma chemistry in addition to He excited species. Lines selection of the emitting species are determined in terms of their order of magnitude within their spectral systems. Experimental conditions are as follows: HV amplitude: 7.5 kV; pulse repetition frequency: 5 kHz; helium gas flow rate: 5 L/min; pulse width: 500ns.

The amyloid fibrils in solution are placed into small tubes (0.2mls) or glass slides and exposed to the plasma pencil for varying lengths of time (up to 10 minutes). After exposure the fibrils are immediately fixed onto 400 mesh formvar coated copper grids for analysis by electron transmission microscopy. Figure 27a shows mature intact α-synuclein fibrils, while Figure 27b shows the morphology of fibrils after 6 minutes exposure to the plasma. It clearly shows that a 6 minutes exposure induces severe damage to the fibril and causes extensive breakage. It is of note to mention that evidence of breakage starts showing up after only 2 minutes exposure to the plasma. Although preliminary, these are extremely important results as this methodology provides a facile and novel mechanism whereby amyloid fibrils can be easily destroyed. Non-equilibrium plasmas such the one generated by the plasma pencil are sources of reactive oxygen species, ROS (such as atomic oxygen and superoxides) and reactive nitrogen species, RNS (such as NO_x) which are known to chemically denature cellular lipids and proteins. So we expect that under plasma exposure the fibrils undergo chemical reactions that compromise their structural as well as chemical integrity.

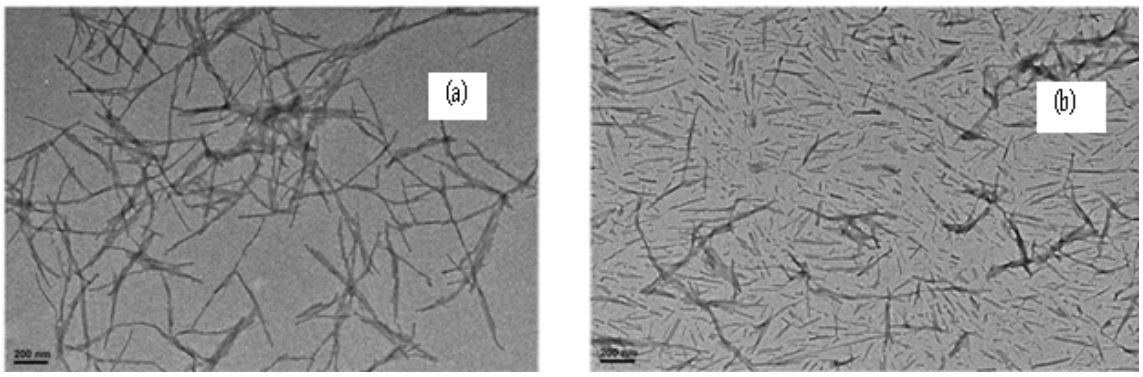

Fig. 27 (a) TEM image of mature intact α-synuclein fibrils; (b) TEM image of the fibrils after 6 minutes exposure to the plasma plume, showing clear evidence of extensive breakage.

The fact that amyloid fibrils are the cause behind such debilitating disease as Parkinson and probably also Alzheimer's makes these results of even greater relevance. However, what remains to be tested is the cytotoxicity of plasma with regard to neurons/neuronal cells. Although studies on other type of eukaryotic cells have shown that low power doses of cold plasma do not cause them irreversible damage to date there are no known tests on neurons/neuronal cells. We also need to determine if the broken fibrils re-associate and are benign to brain cells (not cytotoxic or induce propagation). It will also be very interesting and key to elucidate if the broken fibrils are taken up by microglial cells thus providing a mechanism for how the body may eliminate broken fibrils. The outcome of such tests is of utmost importance if plasma is to be used as a therapy against diseases caused by amyloid fibrils. If the fibrils are indeed chemically altered by the plasma (still to be determined experimentally) they may not be able to re-assemble and their smaller units (broken by the plasma) may not be cytotoxic as those obtained by mechanical agitation, for example. These are in fact important issues that need to be carefully investigated.

Generation of a Large Volume Diffuse Plasma: *Investigating the plasma bullet propagation under controlled pressure and conditions leading to a diffuse operational mode*

To date the plumes generated by plasma jets have been emitted in ambient air at atmospheric pressure. This was motivated by the fact that atmospheric conditions were desired for most applications. In this work, as a departure from this scenario, we investigate the behavior of the plasma plume in a case where the atmosphere in which the plume propagates can be controlled in terms of pressure and contents. Figure 28 is a schematic illustrating what we embarked on investigating. The device generating the plasma jet, tube reactor, consists of a cylindrical acrylic tube with 3 mm inner diameter and two copper foil electrodes wrapped around the tube (see Figure 29). The electrodes are separated by a distance of 15 mm. Helium as a working gas is fed by a mass flow meter (Bronkhorst High-Tech) with an adjustable flow rate. An 8 kV high voltage pulse, 2 μs in width is applied with a 5 kHz repetition rate during all experiments. The acrylic tube which makes the body/housing of the jet source is inserted into one end of the long arm of a cross-shaped large Pyrex chamber. The remaining ports of the Pyrex chamber are used to connect a vacuum pump, a view port (equipped with a fused silica window),

and a vacuum gauge. The pressure inside the chamber is controlled by regulating the gas in-flow and evacuation rate.

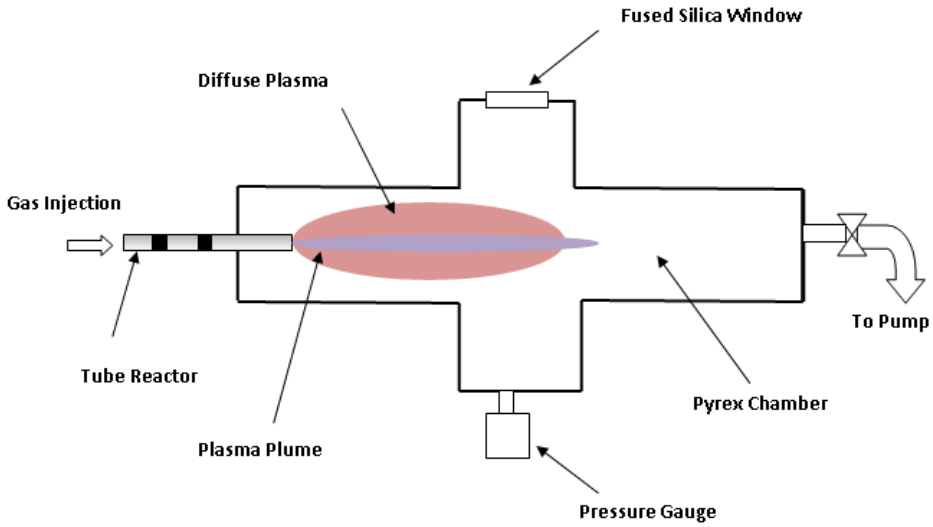

Fig. 28 Experimental setup, showing how a plasma jet is introduced into a Pyrex chamber where pressure can be controlled. The length of one arm of the cross-shaped chamber is 45 cm while that of the second arm is 40 cm.

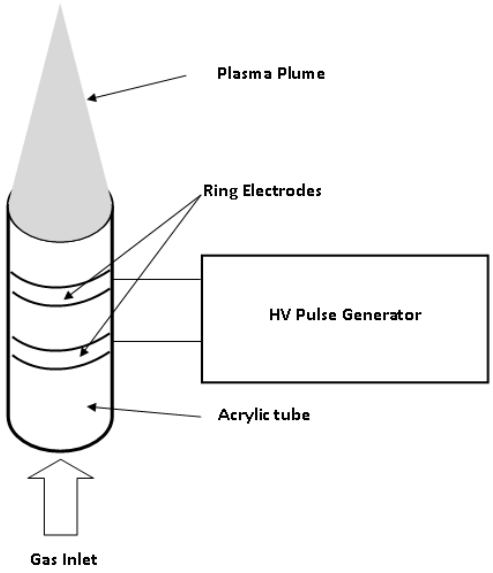

Fig. 29 Schematic of the jet source/generator, the tube reactor, which is used to inject a plasma jet into a Pyrex chamber.

It was shown in our prior work that the plasma plumes are the foot print of a train of plasma packets/bullets that travel within the helium channel at supersonic speeds [13], [14]. The propagation of these bullets was explained with a photoionization model similar to that of

cathode directed streamers [8]. In addition, we showed that the bullets travel within the helium channel then quench when the helium mole fraction falls below a certain value, as it mixes with air [14]. Therefore, controlling the helium flow (for example laminar versus turbulent) affects directly the plume stability and length. In the following experiments, the plume/jet is injected into a chamber where the background pressure can be controlled. Thus, by lowering the pressure, less air molecules will be interacting with the helium flow and a longer helium channel can be achieved. However, we discovered that the behavior of the plume is much more complicated as the pressure changes. In fact, from atmospheric pressure to about 200 Torr, the plume increases relatively slightly in length. Below a pressure of 200 Torr and down to 70 Torr, we observed a rapid increase in the length of the plasma plume. However, below 70 Torr, the length of the plume starts decreasing rather quickly while at the same time the plasma starts expanding in all directions, starting at the tip of the acrylic tube inside the chamber. Figure 30, a plot of plume length versus pressure, illustrates the above observations.

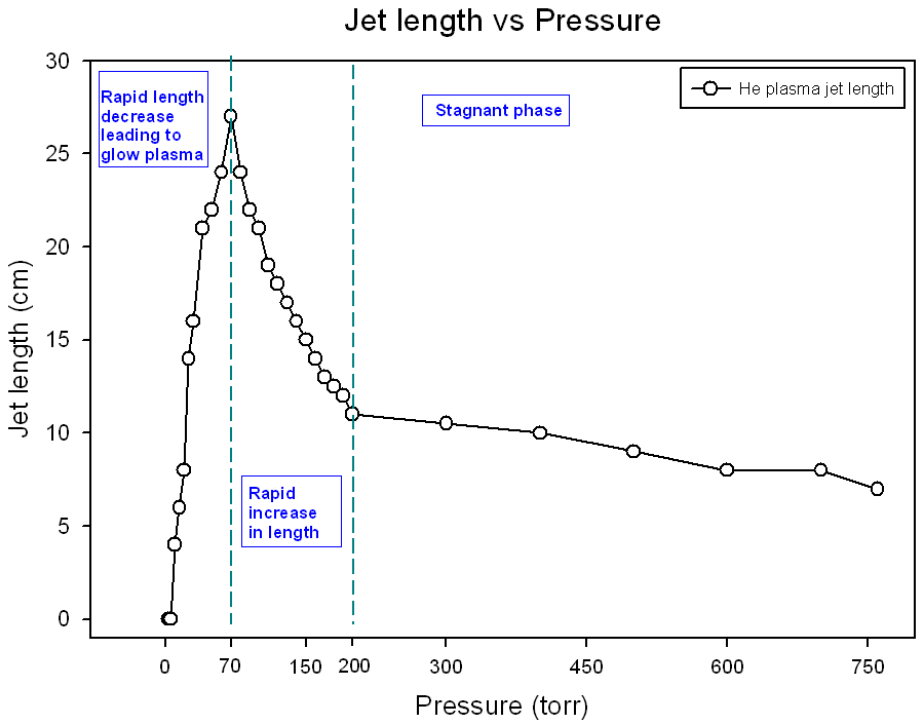

Fig. 30 Plasma plume length versus pressure inside the chamber, showing three distinct phases of operation.

Figure 31, which shows photographs of the plasma plume/jet inside the chamber at 3 different pressures, 760 Torr, 180 Torr, and 75 Torr, illustrates well the dramatic increase of the plume length for pressures below 200 Torr but above 70 Torr (the photo of the plume at 760 Torr is used a reference). The plasma plume/jet length reaches up to 25 cm at a pressure of 75 Torr. This is due to the fact that the ratio of helium mole fraction to that of air stays above the quenching threshold for longer distances.

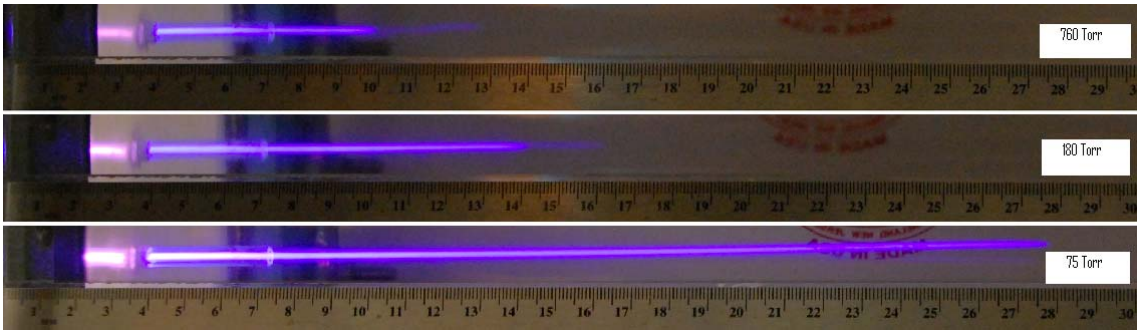

Fig. 31 Plasma plume inside the Pyrex chamber at three pressures: 760, 180, and 75 Torr. The voltage pulse amplitude and width, for this figure and the remaining figures, are 8 kV and 2 μs respectively.

Figure 32 shows the discharge current at the three indicated pressures in the chamber along with the applied high voltage pulse. The peak amplitudes of the current increase as the pressure decreases indicating plasmas with higher densities of electrons and ions. Another phenomenon is observed in this figure as current peaks' temporal position shifts for both the primary and secondary discharges. Primary and secondary discharges are characteristics of pulsed plasma sources of the dielectric barrier type [15]. The primary discharge ignites at the rising edge of the voltage pulse and the secondary discharge occurs at the falling edge [15], [16]. Figure 32 shows that the primary and secondary discharges take place earlier with decreased pressure. One possible explanation for this can be attributed to the fact that breakdown voltage of the working gas (helium in this case) decreases with reduced pressure (decreasing pd from about 1000 Torr-cm to about 100 Torr-cm), in accordance with Paschen's Law. Due to the reduced breakdown strength of the gas and an applied pulse with a finite rise time (~30ns), electrical breakdown can happen earlier at lower electric fields.

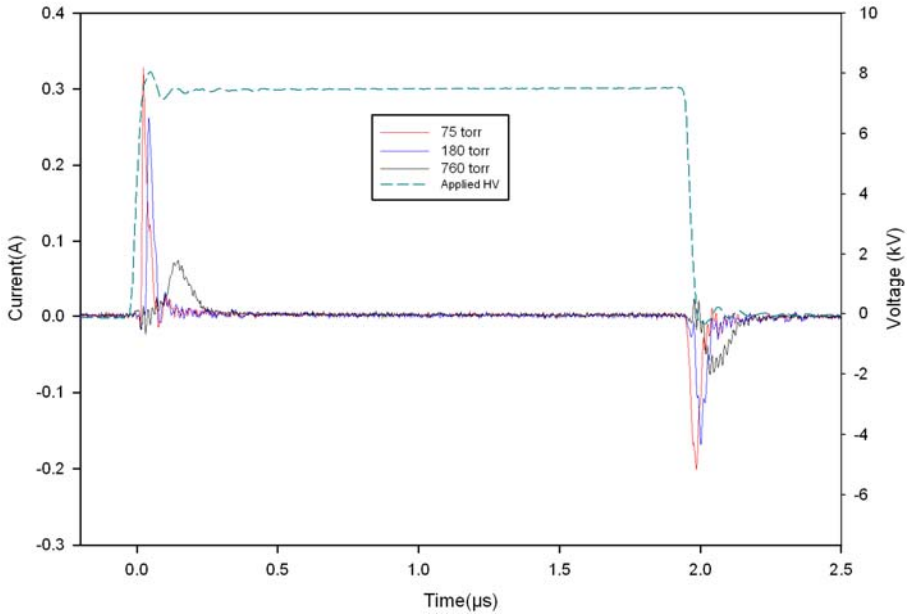

Fig. 32 Current-voltage characteristics under three pressure conditions: 760, 180, and 75 Torr.

When the pressure in the chamber is lowered below 70 Torr, instead of seeing an additional lengthening of the plume, a dramatic decrease in the length takes place. At the same time, starting at the tip of the acrylic tube, plasma starts to expand in all directions inside the chamber, especially when the pressure reaches the 20-25 Torr range. Figure 33 is a photograph illustrating the above visual observations. The image in Figure 6, which was taken at a pressure of 18 Torr, shows clearly a shorter plume (as compared to the 75 Torr case) while a diffuse plasma is expanding from the tip of the acrylic tube.

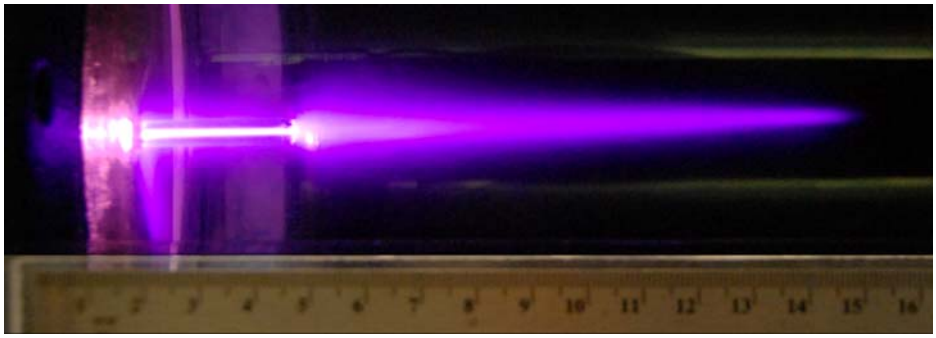

Fig. 33 Photograph showing a shorter plume and an expanding diffuse plasma at the tip of the acrylic tube. The pressure is 18 Torr.

Figure 34 a & b are images taken with an intensified CCD camera (DiCam-Pro ICCD) that show the early onset of this transition. These images are 3 ns snapshots taken at 1.34 μs and 2.2 μs following the applied pulse showing the plasma spreading from the tip of the acrylic tube to the rest of the Pyrex chamber as the plume length decreases. Further lowering the pressure to 10 Torr leads to half the volume of the chamber filling with plasma while at pressures around 2 – 3 Torr plasma fills almost ¾ of the chamber. Below 2 Torr the entire volume of the chamber fills up with uniform and diffuse plasma. Figure 35 is a long exposure picture showing this uniform plasma that has filled almost the entirety of the chamber.

(a)

(b)

Fig. 34 ICCD images of the expanding plasma (a) at 1340 ns; (b) at 2200 ns. The pressure is 10 Torr.

Fig. 35 Long exposure photograph showing diffuse plasma filling the entire Pyrex chamber. The jet source (tube reactor) is visible to the far left.

The sudden shortening of the plume, immediately followed by the ignition of a large volume uniform plasma is an intriguing new observation and constitutes an interesting transition mode (from jet to large volume diffuse plasma) that beckons further detailed investigations which can lead to various interesting applications. The photoionization model proposed by Lu & Laroussi [8] predicts that the plasma would extend in all directions under low pressure conditions. This is what eventually happens, but it only becomes visually apparent when the pressure is below about 75 Torr. At pressures between 760 and 75 Torr, according to the images of the plasma jet, a more or less distinct helium channel exists (less as the pressure approaches 75 Torr) and the plasma jet remains mainly confined in the helium gas channel. When the jet length decreases an expansion of plasma is observed at the tip of the acrylic tube inside the chamber. This observation suggests that with the increased percentage of helium in the chamber compared to the background air, plasma is no longer strictly sustained in a jet phase, but rather in a diffuse fashion. At pressures below 20 Torr this expansion takes over the jet phase as only diffuse plasma is observed. Photons at these pressures are able to ionize the surrounding gas in all directions. This, in combination with diffusion, leads to a non-jet-like diffuse plasma as illustrated by the images shown in this manuscript. The transition from a jet to a large volume diffuse plasma also causes a variation in the plasma bullet shape as seen in the ICCD images. Under these transitional conditions the plasma bullet takes a cometary/arrow shape as it expands inside the Pyrex chamber. This is quite different from the previously reported bullet structure that was observed when plasma jets/plumes were launched into ambient room air.

Other Activities of the P.I.

During the third year of performance of this project, the PI has been involved in various scholarly activities. He organized a minicourse on plasma medicine and healthcare which took place at ICOPS 2012 in Edinburgh, UK. He served as a Guest Editor of a special issue of *Plasma Processes & Polymers* on Plasma Sterilization and Decontamination (Vol. 9, No. 6, 2012). The PI was a member of the Scientific Organizing Committee of two major meetings: The International Symposium on Plasma Chemistry, which took place in Philadelphia, PA, July 2011 and the Fourth International Conference on Plasma Medicine (ICPM-4), which was held in Orleans, France, June 2012. In addition, the PI was a Technical Area Coordinator of ICOPS 2011 and ICOPS 2012. In May 2012 the first book dedicated to the new emerging multidisciplinary field of "Plasma Medicine" was published by Cambridge University Press. Laroussi was the main author and the main editor of this book.

References Cited

[1] B. Eliasson and U. Kogelschatz, *IEEE Trans. Plasma Sci.* **19** 309, 1991.

[2] R. Dorai and M. J. Kushner, *J. Phys. D: Appl. Phys.* **36** 666, 2003.

[3] M. Laroussi , *IEEE Trans. Plasma Sci*. **24** 1188, 1996.

[4] M. Laroussi, *Plasma Proc. Polym*. **2** 391, 2005.

[5] E. E. Kunhardt, *IEEE Trans. Plasma Sci*. **28** 189, 2000.

[6] U. Kogelschatz, *IEEE Trans. Plasma Sci.* **30** 1400, 2002.

[7] M. Laroussi and X. Lu, *Applied Physics Letters* **87**, 113902, (2005).

[8] X. Lu and M. Laroussi, *J. Appl. Phys*. **100**, 063302, (2006).

[9] F. Chiti and C. M. Dobson *Ann. Rev. Biochem.* **75** 333 (2006).

[10] C. M. Eakin and A. D. Miranker *Biochimica Biophysica Acta* **1753** 99 (2005).

[11] F. Chiti, P. Webster, N. Taddei, A. Clark, M.Stefani, G. Ramponi, and C. M. Dobson, *Proc. Natl. Acad. Sci. USA* **96** 3590 (1999).

[12] G. B. Irvine, O. M. El-Anof, G. M. Shankar, and D. M. Walsh, *Mol. Med.* **14** 451 (2008).

[13] N. Mericam-Bourdet, M. Laroussi, A. Begum, E. Karakas, *J. Phys. D: Appl. Phys.* **42**, 055207, (2009).

[14] E. Karakas, M. Koklu, M. Laroussi, *J. Phys. D: Appl. Phys*. **43**, 155202, (2010).

[15] M. Laroussi, X. Lu, V. Kolobov, and R. Arslanbekov, *J. Appl. Phys*. **6**, 3028, (2004).

[16] X. Lu and M. Laroussi, *J. Phys. D: Appl. Phys.* **39**, 1127, (2006).

Papers Published or Presented (2009 – 2011)

Journal Papers

M. Laroussi and M. A. Akman, "Ignition of a Large Volume Plasma with a Plasma Jet", *AIP Advances* **1**, 032138 (2011).

E. Karakas, M. A. Akman, and **M. Laroussi**, "Propagation Phases of Plasma Bullets", *IEEE Trans. Plasma Sci.*, Vol. 39, No. 11, pp. 2308-2309, (2011).

C. Douat, M. Fleury**, M. Laroussi**, V. Puech, "Interactions Between Two counter-propagating Plasma Bullets", *IEEE Trans. Plasma Sci*., Vol. 39, No. 11, pp. 2298-2299 , (2011).

M. Laroussi, E. Karakas, and W. Hynes, "Influence of Cell Type, Initial Concentration, and Medium on the Inactivation Efficiency of Low Temperature Plasma", *IEEE Trans. Plasma Sci*., Vol. 39, No. 11, pp. 2960-2961 , (2011).

Y. Sakiyama, D. B. Graves, J. Jarrige, and **M. Laroussi**, "Finite Elements Analysis of Ring-shaped Emission Profile in Plasma Bullets", *J. Appl. Phys.* **96**, 041501, (2010).

E. Karakas, M. Koklu, **M. Laroussi** "Correlation between helium mole fraction and plasma bullet propagation in low temperature plasma jets", *J. Phys. D: Appl. Phys*. **43**, 155202, (2010).

M. Laroussi, A. Fridman, P. Favia, and M. Wertheimer, "Plasma Medicine – second special issue", Vol. 7, No. 3-4, p. 193, (2010).

E. Karakas, **M. Laroussi** " Experimental studies on the plasma bullet propagation and its inhibiton", *J. Appl. Physics* **108**, 063305, (2010).

J. Jarrige, **M. Laroussi**, E. Karakas "Formation and dynamics of the plasma bullets in a non-thermal plasma jet: Influence of the High Voltage Parameters on the Plume Characteristics", *Plasma Sources Sci. Technol.* **19**, 065005, (2010).

E. Karakas, A. Munyanyi, L. Greene, and **M. Laroussi**, "Destruction of a-Synuclein Based Amyloid Fibrils by Low Temperature Plasma Jets", *Appl. Phys. Lett*. **97**, 143702, (2010).

M. Laroussi, "Low Temperature Plasmas for Medicine?", *IEEE Trans. Plasma Sci.*, Vol. 37, No. 6, pp. 714-725, (2009).

N. Mericam-Bourdet, **M. Laroussi**, A. Begum, and E. Karakas, "Experimental Investigations of Plasma Bullets", *J. Phys. D: Appl. Phys.* **42**, 055207, (2009).

A.D. Morris, G. B. McCombs, T. Akan, W. Hynes, **M. Laroussi**, and S. L. Tolle, "Cold Plasma Technology: Bactericidal Effects on *Geobacillus Stearothermophilus* and *Bacillus Cereus* Microorganisms", *J. Dental Hygiene*, Vol. 83, No. 2, pp. 55-61, (2009).

Conference Papers

E. Karakas, J. Jarrige, M. A. Akman, and **M. Laroussi**, "Chemistry of atmospheric pressure low temperature plasma jets for different experimental parameters", *In Proc. IEEE Int. Conf. Plasma Sci*., Chicago, IL, June 2011.

M. Laroussi, E. Karakas, and M. A. Akman, "How the plasma bullet stops propagating", *In Proc. IEEE Int. Conf. Plasma Sci*., Chicago, IL, June 2011.

M. A. Akman and **M. Laroussi**, "Operating Regimes of a Plasma Jet under Variable Pressures", *In Proc. Gaseous Electronics Conference*, Salt Lake City, UT, Oct. 2011.
C. Douat, M. Fleury, **M. Laroussi**, and V. Puech, "Physical properties of colliding microplasma bullets", *In Proc. Gaseous Electronics Conference*, Salt Lake City, UT, Oct. 2011.

E. Karakas, C. Douat, M. A. Akman, and **M. Laroussi**, "Development Stages of Plasma Bullets", *In Proc. 20th Int. Symp. Plasma Chem*., Philadelphia, PA, July 2011.

E. Karakas, A. Mahasneh, M. Lamaster, **M. Laroussi**, G. McCombs, M. Darby, W. Hynes, "Application of Low Temperature Plasma Jets in Dental Hygiene", in *Gordon-Kenan Research Seminar*, July 10-11, 2010, New London, NH.

L. Greene, **M. Laroussi**, A. Munyanyi, E. Karakas, "Destruction of Amyloid Fibrils by the Plasma Pencil ", in *IEEE 37th International Conference on Plasma Science (ICOPS)* , June 20-24, 2010, Norfolk, VA.

E. Karakas, **M. Laroussi**, M. Koklu "Experimental and Modelling Studies of the Plasma Bullet Lifetime", in *IEEE 37th International Conference on Plasma Science (ICOPS)* , June 20-24, 2010, Norfolk, VA.

A. Begum, E. Karakas, **M. Laroussi**, "Investigations of the Plasma Bullet Velocity by Electrcial and Optical Techniques", in *IEEE 37th International Conference on Plasma Science (ICOPS)* , June 20-24, 2010, Norfolk, VA.

E. Karakas, A. Begum, M. Lemaster, **M. Laroussi**, G. McCombs, M. Darby, and W. Hynes " Experimental Investigations of Plasma Bullets and their Effects on *Streptococcus mutans*", In Proc. 2nd Int. Conf. Plasma Medicine, San Antonio, TX, March 2009. ***Invited Talk***

M. Laroussi, "Plasmas for Biomedical Applications: Interaction Pathways of Low Temperature Plasmas with Biological Cells", In Proc. 40th Annual Meeting of AIP's Division of Atomic Molecular, and Optical Physics, Vol. 54, No. 7, Charlottesville, VA, May 2009. ***Invited Lecture***

A.Begum, E. Karakas, and **M. Laroussi, "**Formation, Propagation, and Contraction of the Plasma Bullets Emitted by a Pulsed Plasma Jet", In Proc. 36th Int. Conf. Plasma Sci., San Diego, CA, June 2009.

Contributing Personnel

Dr. M. Laroussi, P.I., ODU's ECE Dept.
Mr. E. Karakas, PhD student, ODU, ECE Dept.
Mrs. A. Begum, PhD student, ODU, ECE Dept.
Mr. M. A. Akman, MS student, ODU, ECE Dept.
Dr. L. Greene, Biochemist, collaborator, not supported by this grant
Mrs. A. Munyiani, PhD student, collaborator, not supported by this grant